

Diagnosis, prescription and prognosis of a Bell-state filter by quantum process tomography.

M. W. Mitchell¹, C. W. Ellenor¹, S. Schneider² and A. M. Steinberg¹

¹*Department of Physics, University of Toronto, 60 St. George St., Toronto, ON M5S 1A7, Canada*

²*Chemical Physics Theory Group, Department of Chemistry, University of Toronto, 80 St. George St., Toronto, ON M5S 3H6, Canada*

Using a Hong-Ou-Mandel interferometer, we apply the techniques of quantum process tomography to characterize errors and decoherence in a prototypical two-photon operation, a singlet-state filter. The quantum process tomography results indicate a large asymmetry in the process and also the required operation to correct for this asymmetry. Finally, we quantify errors and decoherence of the filtering operation after this modification.

PACS numbers: 42.50-p, 03.67.Mn, 03.67.Pp

Quantum computation promises exponential speedup in the solution of difficult problems such as factoring large numbers and simulating quantum systems [1, 2]. In a quantum computer single- and multiple-qubit operations drive the system through a sequence of highly entangled states before the result is finally measured. A quantum computation is vulnerable to errors and to environmental decoherence, which destroys the entanglement. Characterization of quantum operations including errors and decoherence is a pressing issue for quantum information processing [3], and is possible by the technique of *quantum process tomography* (QPT) [4, 5]. QPT has been demonstrated for single qubits [6, 7] and for mixed ensembles of two-qubit systems [8] in NMR [9]. Here we present QPT of an entanglement-generating two-qubit operation, the partitioning of photons by a beamsplitter in a Hong-Ou-Mandel (HOM) interferometer. Our characterization reveals large imperfections in the process and indicates the appropriate remedy. Finally, we extend the QPT results to predict the accuracy of the process, once repairs are carried out.

Multi-qubit operations on photons, once thought to require very large optical nonlinearities, can now be performed with linear optical elements such as wave-plates and beamsplitters coupled with the highly nonlinear process of photodetection. This idea is exploited in schemes for linear optics quantum computation [10, 11, 12] and to generate multi-photon entangled states [13, 14]. The schemes are probabilistic and employ *post-selection*: the photodetection signals indicate when the correct operation has taken place. The HOM effect plays a central role in these proposals, and itself is a prototypical example of a post-selected multi-qubit operation; it generates correlations and entanglement without optical nonlinearities. The HOM effect has been used to produce entangled states for Bell inequality tests [15, 16] and to make probabilistic Bell state measurements for quantum teleportation and entanglement swapping [17, 18].

In the HOM effect, two photons meeting at a 50/50 beamsplitter can leave by different output ports only if

they are in some way distinguishable [19]. We use photon pairs which are indistinguishable in wavelength, spatial mode and arrival time at the beamsplitter, leaving only the polarization to (possibly) distinguish them. By detecting photons leaving from different output ports, we post-select an entangled polarization state. Ideally, the process acts as a filter for the Bell singlet state $\Psi^- = (HV - VH)/\sqrt{2}$, in which the photons have orthogonal polarizations in any basis. In any real apparatus this process will include errors and decoherence. Using the techniques of QPT, we determine how the polarization state, more specifically the 4×4 density matrix ρ which describes an arbitrary two-photon mixed state, changes in passing the beamsplitter. In general, ρ will change as $\rho^{(in)} \rightarrow \rho^{(out)} = \mathcal{E}(\rho^{(in)})$, where \mathcal{E} is the *superoperator*, a linear mapping from input density matrices to output density matrices. The superoperator completely characterizes the effect on the system, including coherent evolutions, decohering interactions with the environment, and loss.

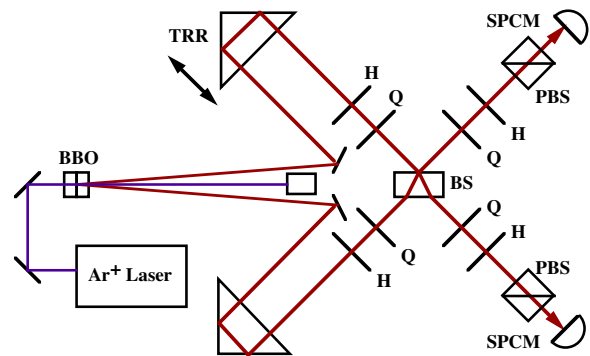


FIG. 1: Schematic of experimental setup. BBO, β -barium borate crystals, H half-wave plate, Q quarter wave plate, BS beamsplitter, PBS polarizing beamsplitter, SPCM single-photon counting module, TRR translatable retro-reflector.

We use a HOM interferometer constructed to produce arbitrary input polarizations and detect arbitrary output polarizations. The experimental setup is shown schemat-

ically in Fig. 1. A 7 mW beam of 351.1 nm light from an argon-ion laser illuminates a pair of 0.6 mm thick β -barium borate crystals, cut for degenerate downconversion at a half-opening angle of 3.3° . Pairs of downconversion photons at 702.2 nm emerge from the crystals vertically polarized. This initial polarization state can be rotated into any input product state by the state preparation half- and quarter-wave plates immediately before the central beamsplitter. The downconversion beams meet the beamsplitter at 45° incidence. The beamsplitter itself [20] consists of a multi-layer dielectric coating on a glass substrate, with an anti-reflection coated back face.

Polarization analyzers consisting of a quarter- and a half-waveplate before a polarizing beamsplitter are used to select an arbitrary product state. Photons which pass the analyzers are detected by single-photon counting modules and individual and coincidence detection rates are registered on a computer. Downconversion beams were aligned to overlap both spatially and temporally on the beamsplitter, giving a HOM dip visibility of $90 \pm 5\%$ for both horizontal and vertical input polarizations. The process tomography measurements described below were performed at the center of this dip.

We prepare 16 linearly independent input states $\{\rho_i^{(in)}\}$ and measure the corresponding outputs $\{\rho_i^{(out)}\}$. The inputs [21] are the pure states $\rho_i^{(in)} = |\psi_i\rangle\langle\psi_i|$ where

$$\{\psi_1, \dots, \psi_{16}\} = \{HH, HV, VV, VH, \\ RH, RVDV, DH, \\ DR, DD, RD, HD, \\ VD, VL, HL, RL\} \quad (1)$$

and the polarizations are horizontal H , vertical V , diagonal $D = (H + V)/\sqrt{2}$, right circular $R = (H - iV)/\sqrt{2}$ and left circular $L = (H + iV)/\sqrt{2}$. A single output $\rho_i^{(out)}$ can be found by making projective measurements onto the sixteen states $\{\psi_j\}$. The coincidence rates for these measurements are $R_{ij} = R_0 \text{Tr}[\rho_i^{(out)} |\psi_j\rangle\langle\psi_j|]$, where R_0 is the constant rate of downconversion at the crystals. Note that we use non-normalized output density matrices, i.e. $\text{Tr}[\rho^{(out)}] \leq 1$, because photon pairs can be lost in the process. Absorption and scattering losses are small, but post-selection necessarily removes a significant fraction of the pairs for most input states.

The measured coincidence rates R_{ij} are shown in Fig. 2. As expected for a filter, the output has similar polarization characteristics for all inputs, but not all are equally transmitted, e.g., HH and VV are blocked. A typical output density matrix, reconstructed using maximum-likelihood estimation [21] is shown in Fig. 3. The large coherence between HV and VH indicates that this is an entangled state, with a concurrence [21, 22, 23] of $C = 0.89$. The HOM effect is acting as an entangled-state filter, but the selected state is clearly not Ψ^- , which has a real density matrix and *negative* off-diagonal ele-

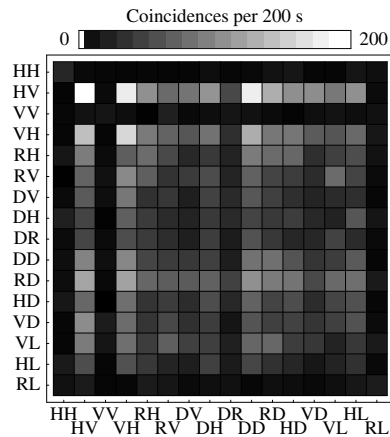


FIG. 2: Coincidence rates. Brightness indicates the count rate observed in a given two-photon polarisation state (horizontal axis) for a given input polarisation state (vertical axis).

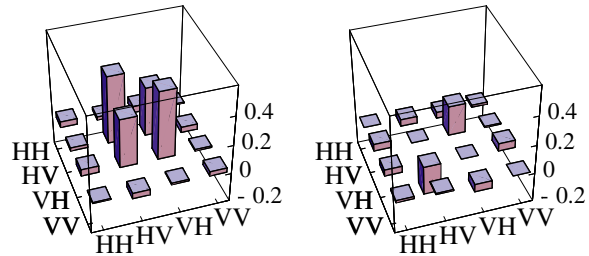


FIG. 3: Output density matrix (normalized) for an input state of HV . Left graph shows $\text{Re}[\rho^{(out)}]$, right graph shows $\text{Im}[\rho^{(out)}]$.

ments.

We can understand this behaviour through the superoperator \mathcal{E} . For clarity, we work in the Bell state basis $\{\Psi^-, \Psi^+, \Phi^-, \Phi^+\}$ where $\Psi^\pm = (HV \pm VH)/\sqrt{2}$ and $\Phi^\pm = (HH \pm VV)/\sqrt{2}$. We use a matrix representation for \mathcal{E} : The density matrix is written as a real 16-dimensional vector $\vec{\rho}$ made from the independent coefficients of the non-normalized density matrix, i.e., $\vec{\rho} = (\rho_{11}, \dots, \rho_{44}, \text{Re}[\rho_{12}], \text{Im}[\rho_{12}], \text{Re}[\rho_{13}], \dots, \text{Im}[\rho_{34}])^T$. The superoperator is represented by a matrix \mathbf{M} which acts as

$$\vec{\rho}^{(out)} = \mathbf{M}\vec{\rho}^{(in)}. \quad (2)$$

In principle, \mathbf{M} could be found from this equation by a simple inversion, since we measured R_{ij} for a basis set $\{\rho_i^{(in)}\}$. This procedure is sensitive to small errors and can produce a non-physical \mathbf{M} , i.e., one which predicts non-physical (mathematically, non-positive semidefinite) $\rho^{(out)}$. Instead, we reconstruct \mathbf{M} by maximum-likelihood estimation within the space of completely positive superoperators, i.e. operators that map physical density matrices to physical density matrices (see e.g. Sudarshan [24] for the mathematical conditions on the mapping between density matrices). The reconstructed \mathbf{M} is

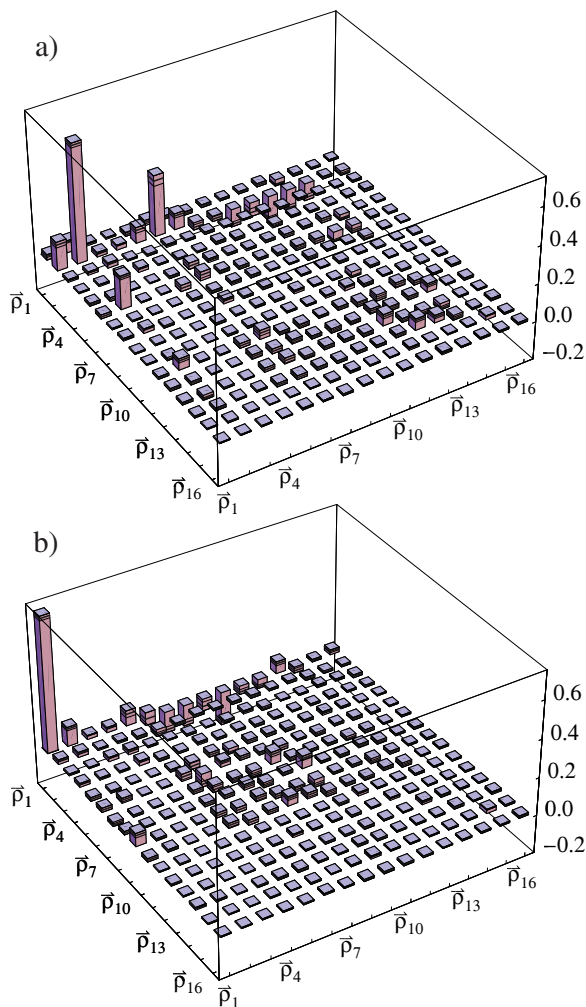


FIG. 4: Reconstructed superoperators for the post-selected HOM process. a) superoperator as measured, b) predicted superoperator after repair. The matrix \mathbf{M} is shown, input density matrix elements at bottom, output elements at left, where the density matrices are represented in vector form (see text). Horizontal stripes on the vertical bars indicate the the best estimated value and the statistical uncertainties.

shown in Fig. 4 a), with error estimates from an ensemble of simulated datasets Poisson distributed around the measured data. This matrix is “normalized” to give $\text{Tr}[\rho_{out}] = 1/4$ when the input is a completely mixed state.

We verify the accuracy of the reconstructed superoperator using the the input states LL and RR , which were not used in the reconstruction process. These states are used as input, both to equation (2) and in the HOM interferometer. In both cases, prediction and the experiment result (again by maximum likelihood reconstruction) agree with fidelity of 97%.

The superoperator \mathbf{M} bears little resemblance to an ideal singlet-state filter, for which $M_{ij} = \delta_{i,1}\delta_{j,1}$. Clearly the process is not performing the intended filtering operation. In fact, it is nearly a projection onto a different

maximally entangled state [25]. Written as a canonical Kraus operator sum [26, 27], the superoperator allows us to find this state directly. In the sum $\mathcal{E}(\rho) = \sum_l \hat{K}_l \rho \hat{K}_l^\dagger$, the leading operator \hat{K}_1 is very nearly a projector onto the state $\Psi_\phi^- \equiv (HV - \exp[i\phi]VH)/\sqrt{2}$ with $\phi = 0.84\pi$. This immediately suggests a way to “fix” the non-ideal beamsplitter. Adding a birefringent phase shifter which takes $VH \rightarrow \exp[-i\phi]VH$ before the beamsplitter and the reverse operation afterward would give (nearly) a single-state filter.

Finally, we can predict the behaviour of this “fixed” operation. The corresponding matrix \mathbf{M} is shown in Fig. 4b). The large (1,1) element indicates the filtering operation and the smaller nonzero elements contribute to decoherence and other errors. These errors presumably arise from imperfect overlap of the downconverted beams and residual imperfections in the beamsplitter. They do not appear to have a simple form, but we can gain some insight from some simple measures, calculated using the superoperator. An unpolarized input (a completely mixed state) gives rise to an output that is 84% Ψ^- , or an average polarization ratio (intensity of Ψ^- versus average intensity of the other three Bell states) of 16:1. This same output is entangled, with a concurrence of $C = 0.70$, sufficient for a Bell inequality violation. Quantifying purity with the linear entropy S_L , which ranges from 0 for a pure state to 1 for a completely mixed state, the process purifies the mixed state from $S_L = 1$ to $S_L = 0.37$. We can also ask how well the repaired filter maintains the coherence of an input. The pure input Ψ^- is passed 75% of the time and emerges largely pure, with $S_L = 0.13$. The state Ψ^+ is 13% passed with $S_L = 0.51$ and Φ^\pm are on average 6% passed with low purity $S_L = 0.88$. Of course, different applications for a singlet-state filter will have different requirements and different figures of merit. The superoperator we have found using QPT is more general, a complete characterization suitable for evaluating any proposed use. It is also, we have seen, a useful diagnostic and predictive tool.

We thank Daniel Lidar, Jeff Lundeen and Kevin Resch for assistance and helpful discussions. This work was supported by the National Science and Engineering Research Council of Canada, Photonics Research Ontario, the Canadian Institute for Photonic Innovations and the DARPA-QuIST program (managed by AFOSR under agreement No. F49620-01-1-0468).

-
- [1] D. P. DiVincenzo, *Science* **270**, 255 (1995).
 - [2] A. Ekert, R. Jozsa, *Rev. Mod. Phys.* **68**, 733 (1996).
 - [3] Quantum information science and technology experts panel, *A quantum information science and technology roadmap*. (2002; <http://qist.lanl.gov>).
 - [4] J. F. Poyatos, J. I. Cirac, P. Zoller, *Phys. Rev. Lett.* **78**, 390 (1997).

- [5] I. L. Chuang, M. A. Nielsen, *J. Mod. Opt.* **44**, 2455 (1997).
- [6] F. De Martini, A. Mazzei, M. Ricci, G. M. D'Ariano, in press (available at <http://arXiv.org/abs/quant-ph/0207143>).
- [7] J. B. Altepeter *et al.* in press (available at <http://arXiv.org/abs/quant-ph/0303038>).
- [8] S. L. Braunstein *et al.* *Phys. Rev. Lett.* **83**, 1054 (1999).
- [9] A.M. Childs, I.L. Chuang, D.W. Leung, *Phys. Rev. Lett.* **78**, 390 (1997).
- [10] E. Knill , R. Laflamme, G. J. Milburn, *Nature* **409**, 46 (2001).
- [11] J. D. Franson, M. M. Donegan, M. J. Fitch, B. C. Jacobs, T. B. Pittman, *Phys. Rev. Lett.* **89**, 137901/1 (2002).
- [12] A. Gilchrist, W.J. Munro, A.G. White in press (available at <http://arXiv.org/abs/quant-ph/0301112>).
- [13] P. Kok, H. Lee, J. P. Dowling, *Phys. Rev. A* **65**, 052104/1 (2002).
- [14] J. Fiurášek, *Phys. Rev. A* **65**, 053818/1 (2002).
- [15] Z. Y. Ou, L. Mandel, *Phys. Rev. Lett* **61**, 50 (1988).
- [16] Y. H. Shih, C. O. Alley, *Phys. Rev. Lett* **61**, 2921 (1988).
- [17] D. Bouwmeester *et al.* *Nature* **390**, p. 575 (1997).
- [18] J.-W. Pan , D. Bouwmeester, H. Weinfurter, A. Zeilinger, *Phys. Rev. Lett.* **80**, 3891 (1998).
- [19] C. K. Hong, Z. Y. Ou, L. Mandel, *Phys. Rev. Lett.* **59**, 2044 (1987).
- [20] CVI Laser Corp. Non-polarizing plate beamsplitter BSNP-702.2-50-0525, 50% reflectance for both s and p polarizations at 702.2 nm.
- [21] D. F. V. James, P. G. Kwiat, W. J. Munro, A. G. White, *Phys. Rev. A* **64**, 052312/1 (2001).
- [22] V. Coffman, J. Kundu, W. K. Wootters, *Phys. Rev. A* **61**, 052306/1 (2000).
- [23] W. K. Wootters, *Phys. Rev. Lett.* **80**, 2245 (1998).
- [24] E. C. G. Sudarshan, P. M. Mathews, J. Rau, *Phys. Rev.* **121**, 920 (1961).
- [25] This may appear surprising, because it is well known that the HOM effect *must* select Ψ^- if the beamsplitter treats H and V polarizations symmetrically. But the beamsplitter used here lacks inversion symmetry (only the front surface is reflective) and this allows a H/V asymmetry. Concretely, when both photons are reflected, one passes through the anti-reflection coated surface twice, while the other does not pass through it at all. If this coating is birefringent the inputs HV and VH will acquire different phase shifts upon double-reflection. As a result, a different state within the Ψ^-, Ψ^+ subspace is selected. To our knowledge, this is the first observation of this asymmetry in the HOM effect.
- [26] M. D. Choi, *Linear Algebr. Appl.* **10**, 285 (1975).
- [27] K. Kraus, *States, effects, and operations: Fundamental notions of quantum theory* (Springer-Verlag, Berlin, 1983).